Final version published as: Tavassoly, O., Sade, D., Bera, S., Shaham-Niv, S., Vocadlo, D. J., & Gazit, E. (2018). Quinolinic Acid Amyloid-like Fibrillar Assemblies Seed α-Synuclein Aggregation. Functional Amyloids in Health and Disease, 430(20), 3847–3862. https://doi.org/10.1016/j.jmb.2018.08.002

Quinolinic Acid Amyloid-like Fibrillar Assemblies Seed α-Synuclein Aggregation

Omid Tavassoly[1,†], Dorin Sade[2,†], Santu Bera[2], Shira Shaham-Niv[2], David J. Vocadlo[1,3] and Ehud Gazit[2,4,5]

*1 - **Department of Chemistry,** Simon Fraser University, Burnaby, British Columbia, Canada V5A 1S6*
*2 - **Department of Molecular Microbiology and Biotechnology,** Tel Aviv University, Tel Aviv 6997801, Israel*
*3 - **Department of Molecular Biology and Biochemistry,** Simon Fraser University, Burnaby, British Columbia, Canada V5A 1S6*
*4 - **Sagol Interdisciplinary School of Neurosciences,** Tel Aviv University, Tel Aviv 6997801, Israel*
*5 - **Blavatnik Center for Drug Discovery,** Tel Aviv University, Tel Aviv 6997801, Israel*

***Correspondence to Ehud Gazit:** Department of Molecular Microbiology and Biotechnology, Tel Aviv University, Tel Aviv 6997801, Israel. ehudg@post.tau.ac.il*

Abstract

Quinolinic acid (QA), a downstream neurometabolite in the kynurenine pathway, the biosynthetic pathway of tryptophan, is associated with neurodegenerative diseases pathology. Mutations in genes encoding kynurenine pathway enzymes, which control the level of QA production, are linked with elevated risk of developing Parkinson's disease. Recent findings have revealed the accumulation and deposition of QA in post-mortem samples, as well as in cellular models of Alzheimer's disease and related disorders. Furthermore, intrastriatal inoculation of mice with QA results in increased levels of phosphorylated α-synuclein and neurodegenerative pathological and behavioral characteristics. However, the cellular and molecular mechanisms underlying the involvement of QA accumulation in protein aggregation and neurodegeneration remain elusive. We recently established that self-assembled ordered structures are formed by various metabolites and hypothesized that these "metabolite amyloids" may seed amyloidogenic proteins. Here we demonstrate the formation of QA amyloid-like fibrillar assemblies and seeding of α-synuclein aggregation by these nanostructures both *in vitro* and in cell culture. Notably, α-synuclein aggregation kinetics was accelerated by an order of magnitude. Additional amyloid-like properties of QA assemblies were demonstrated using thioflavin T assay, powder X-ray diffraction and cell apoptosis analysis. Moreover, fluorescently labeled QA assemblies were internalized by neuronal cells and co-localized with α-synuclein aggregates. In addition, we observed cell-to-cell propagation of fluorescently labeled QA assemblies in a co-culture of treated and untreated cells. Our findings suggest that excess QA levels, due to mutations in the kynurenine pathway, for example, may lead to the formation of metabolite assemblies that seed α-synuclein aggregation, resulting in neuronal toxicity and induction of Parkinson's disease.

Introduction

Millions of people worlwide are afflicted with neurodegenerative diseases, including Alzheimer's disease (AD), Parkinson's disease (PD) and amyotrophic lateral sclerosis, which are characterized by progressive dysfunction of the central nervous system [1–4]. The pathology of these ailments is associated with several amyloidogenic proteins and polypeptides, including β-amyloid in AD [5,6], α-synuclein in PD [7] and TDP-43 in amyotrophic lateral sclerosis [8], which form deposits of β-sheet-rich neurotoxic amyloid aggregates and oligomers in the central nervous system. While not showing any sequence similarity, all of these proteins self-assemble into cytotoxic amyloid structures, suggesting a common underlying mechanism [9]. However, the initial steps leading to the formation and accumulation of these protein aggregates remain elusive [10,11].

Recently, we demonstrated that several metabolites, including phenylalanine, tyrosine, tryptophan, uracil and adenine, can self-assemble and

form structures exhibiting amyloid-like characteristics [12–16]. Each of these metabolites individually accumulates in specific inborn error of metabolism disorders, which all manifest severe neurological abnormalities [17,18]. For example, phenylalanine deposits could be specifically detected using antibodies raised against pre-formed structures, demonstrating their presence in post-mortem brain sections of phenylketonuria patients [14]. Strikingly, it was recently demonstrated that phenylalanine pre-formed fibrils initiated the aggregation of several proteins under physiological conditions [19]. These discoveries expanded the "amyloid hypothesis" to include metabolites in addition to proteins and peptides. The presence of metabolite assemblies in inborn error of metabolism disorders [14,20] and their ability to cross-seed proteins *in vitro* [19] underscore their pathophysiological importance in various diseases. Intriguingly, several neurometabolites have been associated with neurodegenerative pathologies [21–24]. However, no common mechanism underlying the role of these disease-related metabolites has so far been reported [25].

Quinolinic acid (QA) or pyridine-2,3-dicarboxylic acid is an endogenous neurometabolite that has been previously reported to be involved in the pathology of neurodegenerative diseases, including AD, PD and Huntington's disease [26–31]. QA is an intermediate metabolite of the kynurenine pathway that catalyzes transformation of tryptophan into the end-product nicotinamide adenine dinucleotide (NAD^+) (Fig. 1). Through processes that are not fully elucidated, QA can disrupt cell physiology by cytoskeleton destabilization, inducing inflammation, increasing oxidative stress and influencing both autophagy and apoptosis [31]. QA is produced by macrophages and activated microglia [32–34], whereas neurons appear unable to synthesize QA [28,35,36] yet are able to catabolize it [37]. The enzyme 2-amino-3-carboxymuconic semialdehyde decarboxylase (ACMSD) controls the cellular levels of QA by converting a QA precursor metabolite (2-amino-3-carboxymuconate-6-semialdehyde, or ACMS) into the neuroprotective metabolite picolinic acid (PA) [38,39] (Fig. 1). In the absence of ACMSD activity due to mutations in the encoding gene, excess QA precursor metabolite is spontaneously converted to QA. In pathological conditions due to inflammatory

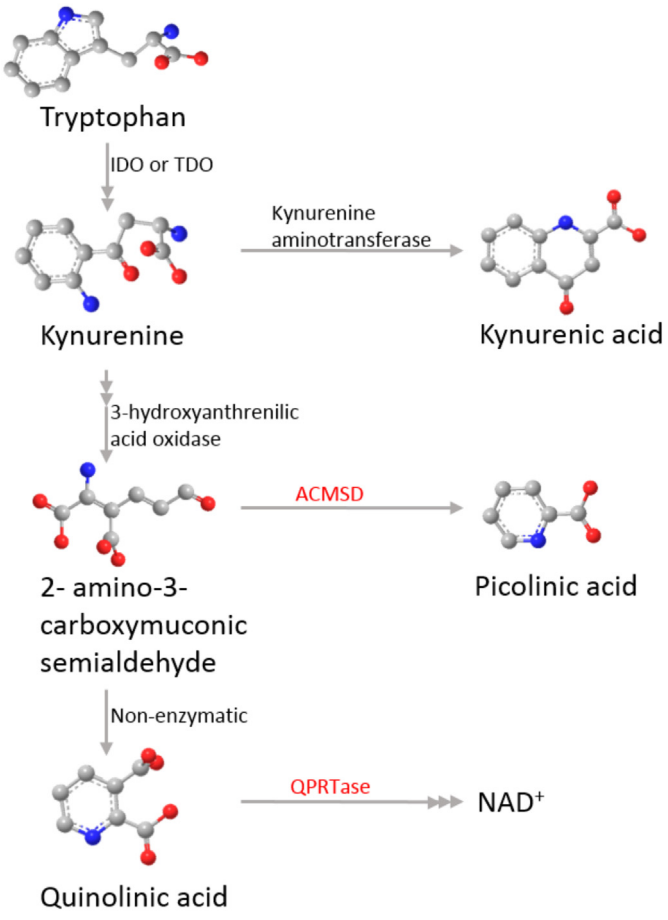

Fig. 1. Simplified diagram of the kynurenine pathway. TDO, tryptophan 2,3-dioxygenase; IDO, indoleamine 2,3-dioxygenases; ACMSD, 2-amino-3-carboxymuconic semialdehyde decarboxylase; QPRTase, quinolinic acid phosphoribosyl transferase; NAD^+, nicotinamide adenine dinucleotide.

responses and reduced ACMSD activity, the kynurenine pathway is over-activated and the production of QA increases [40–42]. Excess QA is released by macrophages and activated microglia and can be internalized by neurons through an unknown molecular mechanism [28,43] leading to its accumulation both inside and outside of neurons [44].

Interestingly, several genome-wide association studies have identified *ACMSD* mutations to be associated with increased risk of PD [25,45–47]. Moreover, *ACMSD* was recently proposed as a novel therapeutic target for PD based on genetic studies showing variations in a locus proximal to the *ACMSD* gene. Furthermore, it has been reported that mutations in *ACMSD* are associated with neurological disease having Parkinsonism-like features [48,49]. These reports collectively suggest that some of the pathology observed in PD pathologies might be initiated by abnormalities in the kynurenine pathway metabolism that give rise to accumulation of QA. These recently identified *ACMSD* mutations may account for PD cases that, until recently, were considered as sporadic in origin. Despite these findings that point to *ACMSD* playing a role as a regulator of PD, the molecular mechanisms underlying its role in the development of PD is still unknown.

Several studies have demonstrated a correlation between QA and AD. In post-mortem brain sections of AD patients, intracellular QA has been detected as punctate structures that co-localize with tau-positive fibrillary structures [28]. QA puncta were also detected in granular deposits within the neuronal soma of cortex from AD patients, which co-localized with neurofibrillary tangles [27,50]. In addition, it has been demonstrated that treatment of human primary neuronal cultures with QA, increases both total and phosphorylated tau [28]. Interestingly, a broad screen of mouse brain samples from an array of mouse strains identified inactivation of *QPRT* as significantly increasing accumulation of β-amyloid [51]. *QPRT* encodes quinolinate phosphoribosyltransferase (QPRTase) (Fig. 1), a neuronal QA catabolic enzyme that allows to maintain low levels of this metabolite within neurons [37,52]. These data suggest a possible mechanism, whereby inhibition of QPRTase activity results in the accumulation of aggregated proteins, possibly due to increased neuronal QA levels.

In this study, we aimed to test our recently presented hypothesis in which we propose that metabolite accumulation and supramolecular structure formation is a fundamental mechanism that may contribute to the initial steps inducing toxicity of amyloids and consequent neurodegeneration [53]. We postulate that these metabolite assemblies can serve as nuclei that cross-seed protein aggregation, thereby accelerating formation of pathological deposits of aggregation-prone proteins such as tau, β-amyloid and α-synuclein. Specifically, regarding the role of QA in PD, we hypothesize that QA accumulation within neurons can trigger its self-assembly and the formation of nucleation seeds. These can, in turn, facilitate the recruitment of soluble α-synuclein monomers into amyloidal aggregates, thus initiating and accelerating the progression and severity of PD and other synucleopathies. Although protein cross-seeding by metabolite assemblies has been demonstrated *in vitro* [19,54], this mechanism has never been explored as an initiator of the neurodegenerative process. Our findings here link α-synuclein pathology with QA accumulation, suggesting a novel target for therapy and drug development.

Results

To demonstrate the formation of QA supramolecular structures and their association with α-synuclein, we performed *in vitro* experiments and cell culture studies. First, we examined whether QA can self-assemble to form higher-order structures (Fig. 2). We dissolved QA at 90 °C in PBS as a physiologically relevant buffer to obtain a homogenous solution after which gradual cooling of the solution resulted in the formation of ordered fibrillary assemblies as assessed by transmission electron microscopy (TEM) (Fig. 2a). QA self-assembly at various concentrations was analyzed using TEM, indicating that the metabolite formed relatively short fibrillary assemblies, homogeneous in length and width and 3–6 nm in diameter as determined from TEM micrographs (Fig. 2a). As a negative control, we examined whether PA, another metabolite of the kynurenine pathway (Fig. 1), can self-assemble. We similarly dissolved and assessed PA solutions using TEM. However, no PA structures could be observed (Fig. S1). Some metabolite fibrillar assemblies were recently reported to exhibit amyloid-like properties, including thioflavin T (ThT) binding and a supramolecular β-sheet-like conformation [12]. Thus, we wanted to test whether QA assemblies display similar characteristics [56–59]. Using fluorometric ThT binding assays, we found that ThT bound to QA assemblies in a concentration-dependent manner, while no detectable binding was observed using a similarly prepared negative control solution of PA (Fig. 2b). Furthermore, we measured the change in quantum yield, considering Rhodamine 6G as a standard. Based on these measurements, we found $\Phi = 0.12$ for blank ThT, which increased to 0.16 upon binding to QA. Given these data, we believe that the binding mechanism is likely an intercalating mechanism, as was suggested for protein and polypeptide amyloids [60–62]; however, this cannot be definitively established without further study.

The powder X-ray diffraction (PXRD) pattern and unit cell parameters of QA-dried fibrils [a = 7.413 (3) Å, b = 12.704 (3) Å, c = 7.826 (3) Å, β = 116.945° (6°)] matched well with the simulated powder diffraction patterns as well as the unit cell parameters obtained from a single crystal structure of QA (a = 7.415 (5) Å,

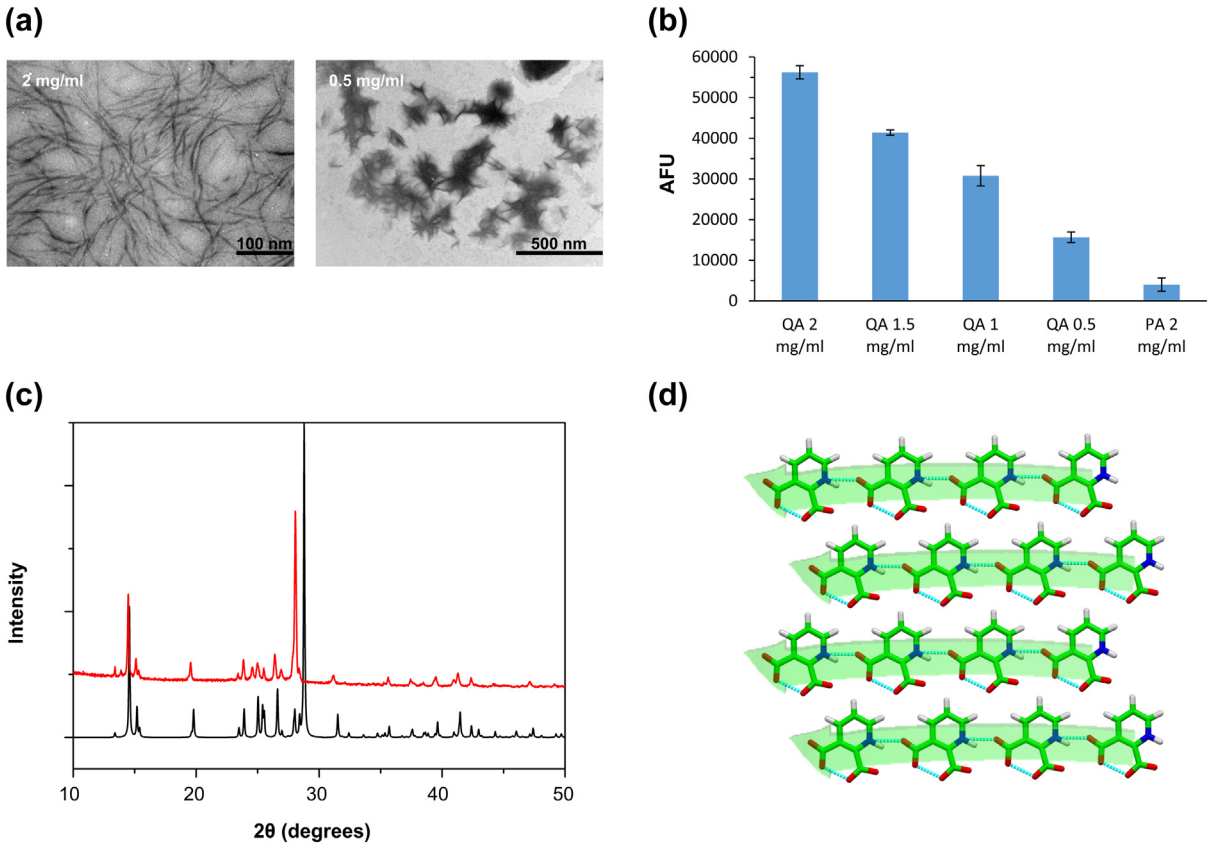

Fig. 2. Characterization of QA assemblies *in vitro*. (a) TEM micrographs obtained 24 h after inducing self-assembly by dissolving QA in PBS at 90 °C followed by gradual cooling. (b) ThT fluorescence emission of QA assemblies. QA (0.5 to 2 mg/ml) and PA (2 mg/ml) were dissolved in PBS at 90 °C, followed by gradual cooling of the solutions. ThT was added to a final concentration of 0.4 μM and emission data at 480 nm (excitation at 450 nm) was measured using spectrofluorometer. AFU, arbitrary fluorescence units. The results represent three independent biological repeats. (c) PXRD patterns and the structure of QA assemblies (2 mg/ml). The solution was centrifuged for 10 min at 6000 rpm and decanted, and the assembled fibers were lyophilized and poured inside a glass capillary. Experimental PXRD pattern was collected for QA fibrils (red) and compared to the simulated PXRD of the crystal structure (black). (d) Crystal structure of QA showing a parallel β-sheet-like structural arrangement. (CCDC no. 1245597) [55].

b = 12.396 (9) Å, *c* = 7.826 (6) Å, *β* = 117.050° (4°)]. These data suggest the presence of similar molecular packing in both the fibrils and single crystals (Fig. 2c) [55]. In the single crystal, each QA molecule was connected through an N(1)–H(4)···O(4) hydrogen bond with the adjacent molecule in the same plane, forming unlimited repeating molecular chain in the crystallographic *a*-direction. Adjacent molecular chains were packed together only by van der Waals interactions approximately along the crystallographic *c*-direction. Each molecular chain can therefore be considered as a single β-strand, reminiscent of a peptide/protein β-strand, which leads one to view the crystal packing of QA as resembling a supramolecular parallel β-sheet-like structural arrangement (Fig. 2d).

Previous studies demonstrated that protein amyloids and metabolite amyloids can be cytotoxic by inducing apoptotic cell death of cultured neuronal cells [12,13,63,64]. We therefore examined the cytotoxicity and apoptotic effect of QA assemblies on cultured human neuroblastoma cells (SH-SY5Y) (Fig. 3). We prepared the assemblies by dissolving various concentrations of QA in culture media, followed by gradual cooling. To evaluate cytotoxicity of QA assemblies, we used a wide range of concentrations of QA to determine their LC_{50} with SH-SY5Y cells following 24 h treatment and using MTT cell viability assay (Fig. 3a). To identify the change in the absorbance resulting from changes in cell viability and to exclude those driven by metabolite assemblies, we used the same concentration of QA assemblies in medium alone as a background measurement that was subtracted from the cell-based viability data. QA assemblies displayed dose-dependent cytotoxicity and caused up to 100% cell death (Fig. 3a). We determined the LC_{50} to be approximately 1.4 mg/ml. We wanted to verify that

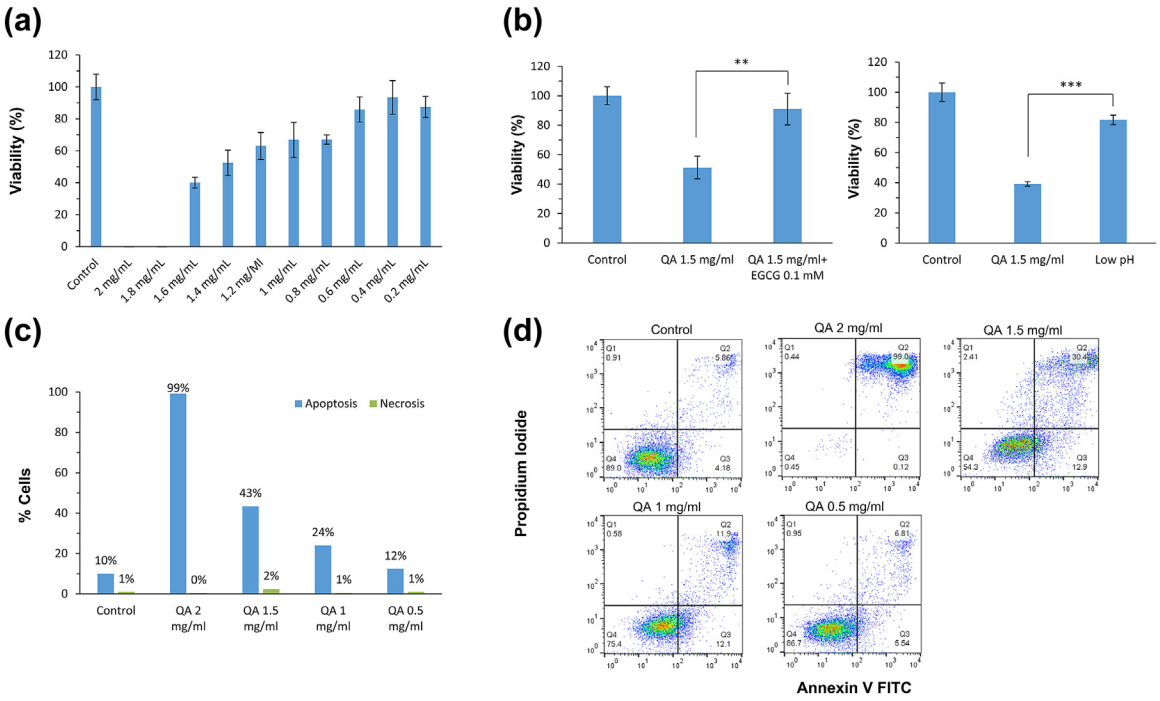

Fig. 3. Cytotoxicity and apoptotic activity of QA assemblies. (a) Cytotoxicity of QA assemblies as determined by MTT cell viability assay. Metabolites were dissolved at 90 °C in cell media followed by gradual cooling of the solution. The control reflects medium without QA, which was treated in the same manner. Treated SH-SY5Y cells were incubated with medium containing QA assemblies for 24 h, followed by the addition of the MTT reagent and extraction buffer. Absorbance was determined at 570/680 nm. The results represent three independent biological repeats. (b) Cytotoxicity of QA assemblies tested by using EGCG to block formation of QA assemblies (left) and evaluation of the effects of low-pH (right). QA (final concentration of 1.5 mg/ml) was similarly dissolved in cell medium (as described in panel a) and mixed with EGCG (0.1 mM) before gradual cooling. Low-pH medium was prepared by adding HCl to reach pH ~6 and was treated in the same manner as the QA-containing medium. The control reflects medium with no metabolites, which was treated in the same manner. The results represent three independent biological repeats. (**$p < 0.01$, ***$p < 0.005$). (c and d) Apoptotic activity studied by annexin V and PI assay. QA was dissolved at 90 °C in SH-SY5Y cell media followed by gradual cooling of the solution. SH-SY5Y cells were incubated with media containing the metabolites at the stated concentrations for 24 h. Control cells were incubated with medium without any addition of metabolites. After incubation, annexin V-FITC and PI were added to the cells, followed by flow cytometry analysis using a single laser-emitting excitation light at 488 nm. (c) Flow cytometry plots of the annexin V/PI double-staining assay. Q1, PI(+) (cells undergoing necrosis); Q2, annexin V-FITC(+) PI(+) (cells in late apoptosis and undergoing secondary necrosis); Q3, annexin V-FITC(+) PI(–) (cells in early apoptosis); Q4, annexin V-FITC(–) PI(–) (live cells). (d) Chart presenting quantification of flow cytometry results. Analyses were performed using the FlowJo software (TreeStar, Version 14). Apoptosis is represented in blue (early + late apoptosis) and necrosis in green. The results represent three independent biological repeats.

cell death was mediated by the QA assemblies and not as a result of an osmotic effect conferred by the high concentration of the metabolite or of pH change of the cell medium. For this purpose, we used the polyphenol epigallocatechin gallate (EGCG), an aggregation inhibitor recently reported to prevent not only protein aggregation but also fibril formation by metabolites [16,65,66]. To verify the inhibition of QA self-assembly by EGCG, the inhibitor (0.1 mM) was added before the gradual cooling of QA solution (1.5 mg/ml). Using TEM analysis, we confirmed that no structures were formed in the mixture of QA with EGCG (Fig. S1). We similarly added EGCG (0.1 mM) to 1.5 mg/ml QA solution in cell medium and treated SH-SY5Y cells for 24 h. MTT assay indicated a significant increase in cell viability compared to QA solution in the absence of EGCG (Fig. 3b, left). Notably, since the addition of EGCG actually increases the monomeric QA concentration, osmotic effect or acidic pH could be ruled out as the main toxic mechanism. Furthermore, since 1.5 mg/ml QA decreases the cell medium pH to 6, we sought to directly test the effect of this pH on cell viability by treating the cells with equivalently low-pH medium for 24 h, followed by MTT cell viability assay (Fig. 3b, right). The viability of the cells grown in low-pH medium was significantly higher compared to cells treated with 1.5 mg/ml QA. Therefore, the presence of QA assemblies in the cell medium is indicated to be the main cause for cytotoxicity.

Next, to better define the mechanism of cytotoxicity and distinguish between apoptosis and necrosis, annexin V and propidium iodide (PI) labeling were used, followed by cell sorting (Fig. 3c, d). Different concentrations of QA assemblies in cell media were prepared as described above, and cultured SH-SY5Y cells were treated with the different QA-containing media for 24 h. As controls, we prepared media without QA. We found similar data using this assay as we had seen using the cytotoxicity assay. The QA solutions caused cell death and stimulated apoptotic activity in a concentration-dependent manner, again up to 100% as indicated by annexin V and PI assay (Fig. 3c, d). These results demonstrate that apoptosis, rather than necrosis, was the main pathway causing SH-SY5Y cell death following treatment with QA assemblies.

We next set out to evaluate the ability of QA assemblies to cross-seed the aggregation of α-synuclein [67]. Monomeric α-synuclein (50 μM) was co-incubated with pre-formed QA seeds for 48 h, and protein aggregation was monitored using a ThT binding assay (Fig. 4a). We found that 30% v/v QA seeds induced α-synuclein aggregation within several hours, while 10% v/v QA seeds showed slower kinetics that eventually reached the same fluorescence signal. Samples of 50 μM α-synuclein in the absence of QA seeds showed significantly slower aggregation kinetics and a weak fluorescence signal (Fig. 4a). Seeding of amyloidogenic proteins by pre-formed fibrils is well established, reporting that solution conditions may affect α-synuclein aggregation [67]. Thus, we used an equivalent solution of low-pH PBS and added it as a potential seeding inducer in the same

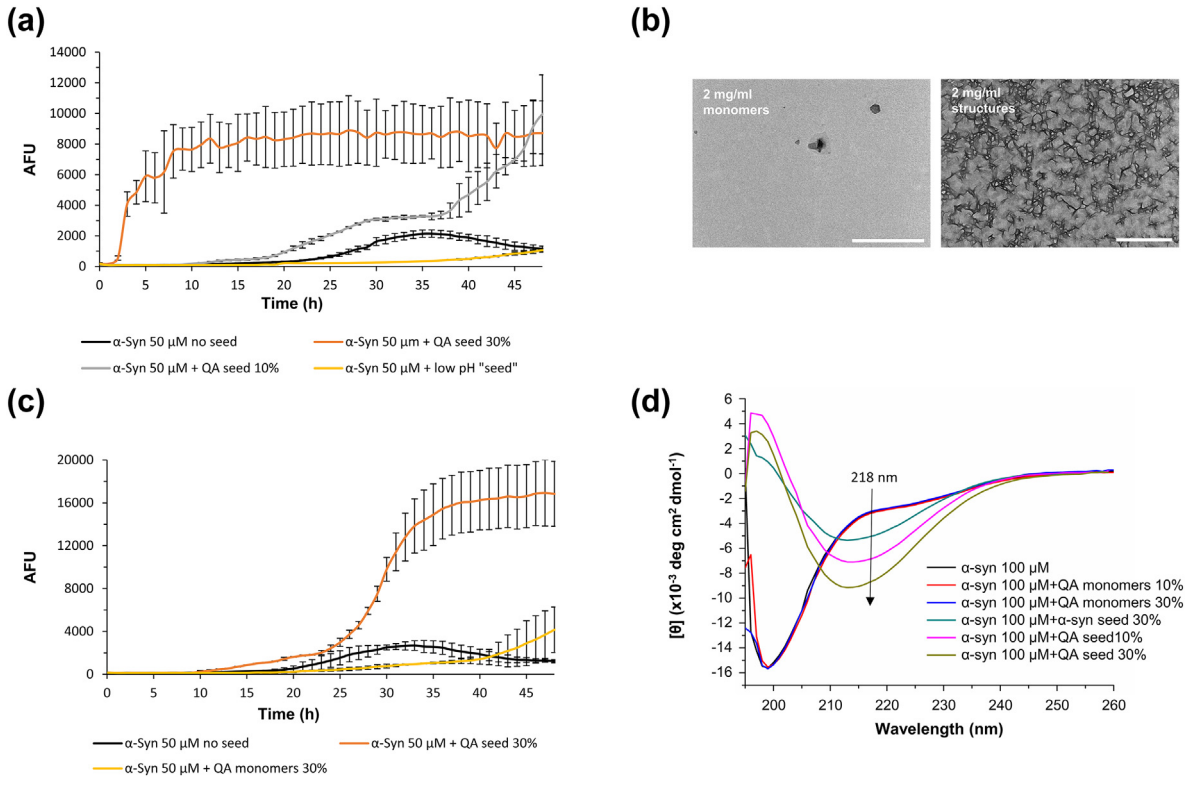

Fig. 4. Cross-seeding of α-synuclein by QA assemblies. (a) Kinetic analysis of the aggregation of α-synuclein in the presence of QA assemblies. α-Synuclein was dissolved in PBS to 70 μM and mixed with 30% or 10% v/v pre-formed QA assemblies (taken from a 2 mg/ml stock sample) or with an equivalent volume of PBS for the "no seed" sample, to a final concentration of 50 μM α-synuclein. Low-pH control was prepared by mixing an equivalent volume of low-pH PBS. Aggregation was monitored using ThT (40 μM) binding assay, over the course of 48 h, at 37 °C with 850 rpm shaking. Blank measurements of samples without α-synuclein were respectively subtracted. The results represent three independent biological repeats. (b) TEM micrographs taken from QA monomers and QA assemblies solutions prepared by dialysis. The scale bar represents 1 μm. (c) Kinetic analysis of α-synuclein aggregation (50 μM) in the presence of QA monomers and QA assemblies (30% v/v taken from 2 mg/ml dialyzed samples). Aggregation was monitored in the same way described in panel a. Blank measurements of samples without α-synuclein were respectively subtracted. The results represent three independent biological repeats. (d) Far-UV CD spectra of α-synuclein (100 μM) in the presence and absence of QA monomers and QA assemblies (10% and 30% v/v taken from 2 mg/ml dialyzed samples) and α-synuclein seed (30% v/v) after 48 h incubation at 850 rpm and 37 °C. The results represent three independent biological repeats.

volume as QA solution in PBS. However, we found that the equivalently low-pH conditions did not affect the aggregation of α-synuclein monomers (Fig. 4a). Next, to validate the cross-seeding effect of QA assemblies, we aimed to examine the seeding of α-synuclein by QA monomers. Since an EGCG control could not be used in a protein aggregation assay [65,66], we used dialysis to separate QA monomers from QA assemblies in a 2 mg/ml solution. The samples were examined using TEM (Fig. 4b), verifying that the monomers fraction did not contain any structures, while the dialyzed fraction of QA assemblies showed the presence of typical structures (Fig. 4b). We examined the ability of dialyzed solutions of QA monomers and QA assemblies (30% v/v) to cross-seed the aggregation of 50 μM α-synuclein (Fig. 4c). In comparison to non-dialyzed QA assemblies (Fig. 4a), the dialyzed assemblies showed slower kinetics of α-synuclein aggregation, while the monomers control had a minor effect, similar to the low-pH control. The slower kinetics may be explained by the fact that during dialysis, small oligomers of QA (pentamers and hexamers) can pass the dialysis pore. The absence of these nucleation seeds in the dialyzed assemblies solution may delay α-synuclein aggregation. To assess potential non-specific effects of QA seeds on protein aggregation in general, we used bovine serum albumin (BSA) as a control protein. We observed no change in the aggregation of BSA in the presence of QA seeds measured using this assay (Fig. S2A). In all cases, background ThT fluorescence in the presence of the metabolites alone was subtracted from all experiments. These observations were supported by TEM imaging of the aggregation end-point (Fig. S2B). We found that samples of α-synuclein exposed to QA seeds that showed a high ThT fluorescence also contained amyloid aggregates with characteristic morphology [68] in electron microscopy experiments (Fig. S2B, bottom), whereas samples that had not been treated with seeds contained low numbers of small amorphous aggregates (Fig. S2B, top). We also evaluated the cross-seeding of α-synuclein by QA assemblies using an independent method in which we monitored the formation of β-sheet-like structures *via* circular dichroism (CD) spectroscopy [69]. The conformational change from random coil to β-sheet-like structure, a defining feature of α-synuclein fibrils [70,71], was studied by monitoring the CD signal at 218 nm, which is characteristic of a β-sheet structure [69,72] (Fig. 4d). We incubated α-synuclein monomers for 48 h with QA assemblies, QA monomers (separated by dialysis) or pre-formed fibrils of α-synuclein as a positive control (Fig. 4d). We found that the CD spectrum of α-synuclein in the absence of seeds was typical of peptides with a random coil conformation [73], showing an intense negative minimum at ~200 nm and a weak negative shoulder at ~218 nm. Similarly, in the presence of QA monomers (30% or 10% v/v solutions obtained by dialysis), there was no change in the random coil conformation of α-synuclein even after 48 h incubation (Fig. 4d). However, in the presence of QA assemblies (30% or 10% v/v) or α-synuclein pre-formed fibrils (30% v/v), α-synuclein monomers underwent fibrillization to form β-sheet-like structures as indicated by the distinctive negative maximum at ~218 nm (Fig. 4d). These data are consistent with ThT binding assay results (Figs. 4a and S2A) and TEM images (Fig. S2B) demonstrating the cross-seeding of α-synuclein by QA assemblies and the induced aggregation of α-synuclein into fibrillar structures, which are composed of mostly β-sheet-like conformation.

Given these findings, we were curious to see whether QA assemblies could seed the aggregation of intracellular α-synuclein within cultured cells. A well-established cell-based fluorescence protein-complementation assay, H4/V1S-SV2, was used for these experiments [74–77]. The H4/V1S-SV2 cell model is a H4 neuroglioma cell line that co-expresses two constructs of α-synuclein, one tagged by the N-terminal half of Venus YFP (V1S) and the other tagged by the C-terminal half of Venus YFP (SV2), both under the tetracycline-controlled transcriptional activation system (Tet-Off induction) [74–77]. Cultures of these cells were treated with QA assemblies and α-synuclein pre-formed fibrils for 48 h. High-content fluorescence imaging analysis was used to measure the extent of α-synuclein aggregation upon treatment with either type of seeds (Fig. 5a, b). We found that QA assemblies strikingly increased the aggregation of intracellular α-synuclein in a concentration-dependent manner. The aggregation was imaged and quantified using ImageXpress Molecular Devices and MetaXpress software based on number, area and intensity of α-synuclein aggregation in nine different non-overlapping fields. Strikingly, we found that the extent of seeding of intracellular α-synuclein aggregation within cells by QA assemblies was comparable to that seen when using the same concentration (0.5 mg/ml) of α-synuclein pre-formed fibrils (Fig. 5a).

A prerequisite for QA assemblies acting directly to seed α-synuclein fibrils within cells is the ability of cells to internalize QA assemblies. Moreover, this seeding hypothesis suggests that QA assemblies should co-localize with cellular α-synuclein fibrils. To test this proposal, we used the H4/V1S-SV2 cell line model and treated these cells with Alexa-Fluor-647-labeled-QA assemblies (QA-647) for 48 h, after which we analyzed the cells by confocal microscopy and observed co-localization of QA-647 and intracellular α-synuclein aggregates (Fig. 5c). The uptake of QA-647 and the co-localization with α-synuclein were similarly observed *via* 3D analysis of treated cells (Fig. S3). Moreover, fibrillation of α-synuclein monomers by QA assemblies and their co-localization were studied *in vitro*. α-Synuclein monomers labeled with Alexa-Fluor-488 were incubated with QA-647 for 48 h, followed by confocal microscopy analysis showing

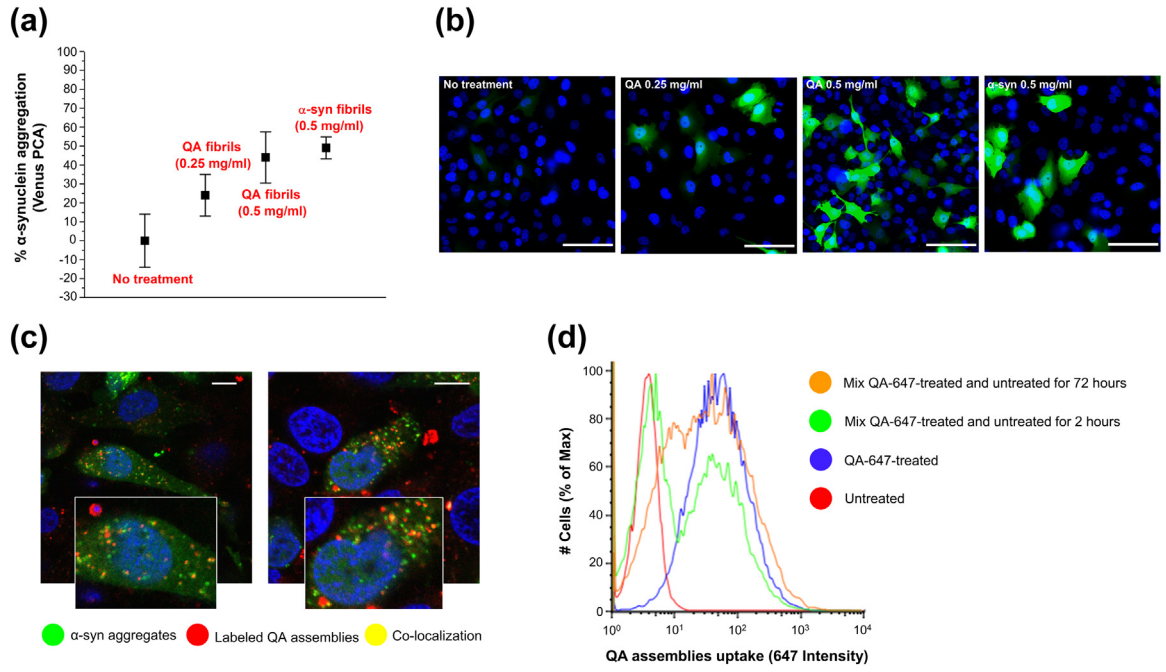

Fig. 5. Induced aggregation of α-synuclein by QA assemblies, co-localization and QA propagation in cell culture. (a, b) High-content cellular analysis of α-synuclein aggregation. (a) Quantification of α-synuclein aggregation 48 h post-treatment using a fluorescent protein-complementation H4/V1S-SV2 cell line (see Materials and Methods). These cells were treated with QA assemblies (0.25 and 0.5 mg/ml) and α-synuclein pre-formed fibrils (0.5 mg/ml) for 48 h. Fluorescence signals from Venus were quantified with automated methods using MetaXpress software (Molecular Devices). Error bars represent ± SD. (b) Representative images of high-content cellular analysis in panel a. The scale bar represents 100 μm. (c) Co-localization of α-synuclein with labeled QA. Confocal images showing QA assemblies (red) and α-synuclein aggregates (green) in H4/V1S-SV2 cell line model, a fluorescent protein-complementation cell line (Venus PCA), 48 h post-treatment with labeled QA-647 at final concentration of 0.5 mg/ml. The scale bar represents 10 μm. The results represent three independent biological repeats. (d) Propagation of labeled QA-647 assemblies. FACS analysis of QA-647 assemblies propagation between SK-N-SH cells. Cells were treated with 0.25 mg/ml of QA-647 assemblies for 24 h and re-plated after washing with PBS and diluted trypsin. Treated and untreated cells were co-cultured for either 72 or 2 h, as a negative control, and Cy5 fluorescence intensity was measured. The results represent three independent biological repeats.

co-localization of QA-647 and α-synuclein-488 aggregates (Fig. S4). This was further supported by the absence of fibrillation or co-localization when labeled α-synuclein was incubated alone, as well as when the mixture of labeled α-synuclein with QA-647 was examined at time zero. Next, we wanted to investigate whether QA-647 assemblies could propagate between cells, as is now well established for amyloids [78–82]. The propagation of QA-647 between cells was measured by co-culturing washed QA-647-treated SK-N-SH cells with untreated cells and monitoring the fluorescence signal of the overall cell population by FACS (Fig. 5d). In this experiment, we treated cells with QA-647 for 24 h, washed and trypsinized them and then co-cultured them with cells that have never been exposed to QA assemblies. As a negative control, we used cells co-cultured for only 2 h, which we judged to be too short for potential spreading of QA assemblies. While the 2 h co-culture showed two distinct separate populations, each resembling the separate treated and untreated populations, the 72 h co-culture showed a broader peak, indicating that QA-647 was passing from QA-treated cells into neighboring untreated cells (Fig. 5d).

Discussion

In this study, we demonstrated that QA, a neurometabolite that has been previously reported to be associated with the pathology of neurodegenerative diseases, can self-assemble into amyloid-like structures. TEM analysis and ThT binding assays indicated that QA forms supramolecular structures. PXRD of QA fibrils supports the known crystal structure of QA single crystals having a structure reminiscent of a supramolecular parallel β-sheet. Furthermore, QA assemblies induced apoptotic cell death and fluorescently labeled QA assemblies were shown to propagate between cells, a prion-like behavior that until now was attributed solely to proteins and polypeptides. Finally, we found that QA seeds facilitated the aggregation of soluble

α-synuclein monomers both *invitro* and in cell-culture, similar to the extent seen upon seeding by α-synuclein pre-formed fibrils. In summary, diverse findings have suggested links between QA accumulation and the enzymes involved in its metabolism to neurodegenerative diseases [28,49,51]. Specifically, in PD, the concentration of QA in cells in pathological conditions has not yet been reported. However, metabolomics studies demonstrated the kynurenine pathway of tryptophan metabolism to be elevated [23,83], consistent with the observations of QA accumulation in amyloid plaques [27,50]. Nevertheless, no specific molecular mechanisms have been deciphered to account for these disparate observations. Our results provide strong support for the hypothesis that QA accumulation may lead to QA assemblies that serve as seeds that can induce the aggregation of α-synuclein, offering a possible molecular mechanism to explain these previous observations linking enzymes regulating QA levels and neurodegeneration. Accordingly, we propose that excess QA, accumulated during disturbed metabolism can form extra- or intra-cellular assemblies, which are most likely not substrates of QPRTase (Fig. 1), as the geometry of its active site recognizes and supports binding of a single QA molecule [84] and would most likely preclude binding of a large assembly. In this mechanism, extracellular QA assemblies are taken up by neurons (or rather intracellularly formed) and serve as a seed to promote α-synuclein aggregation, which is supported by co-localization of QA assemblies with α-synuclein aggregates. Moreover, we reason based on our observations that QA assemblies can propagate between neurons, thereby contributing to the spreading of pathology throughout the brain in a manner that is similar to the phenomenon of prion-like spreading of amyloidogenic fibrils in neurodegenerative diseases [81,85]. Notably in this regard, intrastriatal inoculation of mice with QA causes phosphorylation of α-synuclein, a marker of α-synuclein aggregation, as well as typical pathological and behavioral features of striatonigral degeneration and multiple system atrophy [26,29,86]. These data suggest that cell-to-cell propagation of QA assemblies occurs and may further contribute to cross-seeding of proteins, which in turn drives neurodegeneration. Our proposed mechanism of action for QA ultimately requires *in vivo* validation in PD animal models. However, eventual validation of this QA seeding hypothesis and its role in neurodegeneration will present new opportunities within the field of neurodegeneration and expand our current understanding of the mechanisms behind disease progression. Such an advance may in turn enable new opportunities for the development of therapeutics to treat PD, such as increasing the activity of QPRTase and ACMSD (Fig. 1) or blocking QA fibril formation and its cellular uptake. Finally, this line of research may offer a new paradigm regarding the molecular basis of neurodegenerative diseases.

Materials and Methods

Materials

Recombinant wild-type α-synuclein was purchased from Alexotech (AS-600-10). QA, PA and EGCG were purchased from Sigma (purity ≥99%). Fresh stock solutions of QA assemblies were prepared by dissolving the metabolite at 90 °C in PBS or in cell culture media at various concentrations, to obtain monomeric solutions of the metabolite, followed by gradual cooling of the solution.

TEM

QA or PA was dissolved at 90 °C in PBS at various concentrations followed by gradual cooling of the solution. For EGCG control, QA solution was mixed with the inhibitor (0.1 mM) before gradual cooling. Samples prepared by dialysis were immediately loaded. Subsequently, 10 µl samples were placed on 400-mesh copper grids. After 2 min, excess fluids were removed. Samples were viewed using a JEOL 1200EX electron microscope operating at 80 kV. Diameter calculation of metabolite amyloidal fibers was performed by measuring five fibers from three different QA assemblies images.

Separation of QA assemblies and QA monomers by dialysis

QA assemblies and QA monomers were prepared as previously described for chemical fibrils [87]. To purify QA monomers, a high-throughput dialysis tube (Sigma, 1 kDa MWCO) was filled with PBS and incubated overnight at 4 °C in 1 L of pre-formed QA assemblies (2 mg/ml). The sample inside the dialysis tube was characterized as QA monomers. To purify QA assemblies, the dialysis tube was filled with pre-formed QA assemblies (2 mg/ml) and incubated overnight at 4 °C in 1 L of PBS. The sample inside the dialysis tube was characterized as QA assemblies.

ThT fluorescence

QA was dissolved at 90 °C in PBS at various concentrations ranging from 0.5 to 2 mg/ml, and PA was similarly dissolved to 2 mg/ml, followed by gradual cooling of the solutions. One hundred microliters of ThT solution (4 µM in PBS) was mixed with 900 µl of QA or PA solution and immediately transferred into a rectangular quartz fluorescence cuvette with an optical path length of 10 mm (Hellma Analytics, Müllheim, Germany). Fluorescence was measured using a Fluorolog-3 spectrofluorometer (Horiba Jobin Yvon, Edison, NJ, USA). The excitation wavelength was set to 450 nm, emission was recorded at 480 nm, with excitation, and emission slits of

5 nm. Each experiment was repeated three times. The data points are presented as mean ± SD.

PXRD

QA (2 mg/ml) was dissolved at 90 °C in PBS followed by gradual cooling of the solution. The assembled fibers were lyophilized and poured inside a glass capillary 0.5 mm in diameter. X-ray diffraction was collected using Bruker D8 Discover theta/theta diffractometer with liquid-nitrogen-cooled intrinsic Ge solid-state linear position detector. The cell parameters were determined using the GSAS-II software [88]. The diffraction pattern was analyzed using the Rietveld method with a final RBragg = 5.8% [89]. The peaks were indexed by monoclinic unit cell with a = 7.413 (3) Å, b = 12.7044 (3) Å, c = 7.826 (3) Å and β = 116.945° (6°).

Cell cytotoxicity experiments

SH-SY5Y cells (ATCC CRL-2266) (2×10^5 cells/ml) were cultured in DMEM/Nutrient Mixture F12 (Ham's; 1:1; Biological Industries) supplemented with 10% fetal bovine serum (FBS) in 96-well tissue microplates (100 µl per well) and allowed to adhere overnight at 37 °C. Half of each plate was plated with cells, with the other half later serving as a control for the solutions alone. The treatment solutions were prepared as follows: QA was dissolved at 90 °C in cell media without FBS, at various concentrations ranging from 0.2 to 2 mg/ml, followed by gradual cooling of the solutions. Cells media was replaced and cells were treated with the solutions (100 µl per well), followed by overnight incubation at 37 °C. Control cells were incubated with medium that was treated in the same manner without any addition of QA. For EGCG control, QA (final concentration of 1.5 mg/ml) was similarly dissolved in cell media and mixed with EGCG (final concentration of 0.1 mM, stock solution dissolved cell media) before gradual cooling. For pH control, 10 ml of cell medium was supplemented with 15 µl HCl (32%; same pH of 1.5 mg/ml QA in cell medium) to reach pH ~6. The low-pH medium was treated in the same manner as QA samples in cell media. Cell viability was evaluated using the 3-(4,5-dimethylthiazolyl-2)-2,5-diphenyltetrazolium bromide (MTT) assay. Briefly, 10 µl of 5 mg/ml MTT dissolved in PBS was added to each well. After a 4 h incubation at 37 °C, 100 µl of extraction buffer [20% SDS dissolved in a mixture of 50% DMF and 50% DDW (pH 4.7)] was added to each well, and the plates were further incubated at 37 °C for 30 min. Finally, color intensity was measured using an ELISA reader at 570/580 nm. The data points are presented as mean ± SD. Each experiment was repeated three times. For EGCG and pH controls, two-tailed Student's t test was performed when two groups were compared.

Flow cytometry for apoptosis studies

SH-SY5Y cells were seeded at 2×10^5 per well in 6-well plates and were allowed to adhere overnight at 37 °C. The treatment solutions were prepared as follows: QA was dissolved at 90 °C in DMEM/Nutrient Mixture F12 (Ham's; 1:1; Biological Industries) without FBS at various concentrations ranging from 0.5 to 2 mg/ml, followed by gradual cooling of the solution. Cells were treated with the solutions (3 ml per well), followed by overnight incubation at 37 °C. Control cells were incubated with medium that was treated in the same manner without any addition of metabolites. The apoptotic effect was evaluated using the MEBCYTO Apoptosis kit (MBL International), according to the manufacturer's instructions. Briefly, the adherent cells were trypsinized, detached and combined with floating cells from the original growth medium. Cells were then centrifuged and washed once with PBS and once with binding buffer. Cells were subsequently incubated with annexin V–FITC and PI for 15 min in the dark, resuspended in 400 µl binding buffer and analyzed by flow cytometry using a single laser-emitting excitation light at 488 nm. Data from at least 10^4 cells were acquired using BD FACSort and the CellQuest software (BD Biosciences). Analysis was performed using the FlowJo software (TreeStar, version 14). Each experiment was repeated three times.

In vitro seeding of recombinant α-synuclein by QA assemblies

QA (2 mg/ml) was dissolved at 90 °C in PBS followed by gradual cooling of the solution. Recombinant α-synuclein (Alexotech) was dissolved in PBS to a concentration of 70 µM. The monomeric protein was mixed with the pre-formed 30% v/v or 10% v/v QA assemblies (taken from 2 mg/ml stock solution), or with an equivalent volume of PBS as a control, to a final concentration of 50 µM α-synuclein. For low-pH control, 10 ml of PBS was supplemented with 12 µl HCl (32%) to reach pH ~3 (same pH of 2 mg/ml QA in PBS). An equivalent volume of low-pH PBS was mixed with α-synuclein to the same final concentration. As an additional control, α-synuclein was mixed with QA monomers or pre-formed QA assemblies (10% and 30% v/v taken from 2 mg/ml dialyzed samples, see dialysis above). BSA solution (70 µM) was similarly prepared and mixed with QA assemblies (30% v/v) under the same conditions as α-synuclein. In all experiments, the total sample volume was 140 µl (100 µl protein solution + 14/40 µl QA seed and + PBS up to 140 µl). ThT was added to a final concentration of 40 µM and aggregation was monitored using Tecan™ SPARK 10 M fluorescence plate reader, over the course of 48 h, at 37 °C with 850 rpm shaking. Blank measurements of metabolite only (without α-synuclein or BSA) were, respectively, subtracted. The data

points are presented as mean ± SD. Each experiment was repeated three times.

CD

CD spectra were recorded as previously described [73,90]. Briefly, recombinant α-synuclein (Alexotech) dissolved in PBS to a final concentration of 100 μM was incubated with QA monomers or pre-formed QA assemblies (10% and 30% v/v taken from 2 mg/ml dialyzed samples, see dialysis above). As control, 30% (v/v) seed of α-synuclein pre-formed fibrils was used. Samples were prepared on an Eppendorf ThermoMixer® C at 37 °C with shaking at 850 rpm for 48 h. In all experiments, the total sample volume was 200 μl (100 μl protein solution + 20/60 μl QA seed and + PBS up to 200 μl). The final products were diluted in 10 mM sodium phosphate buffer (pH 7.4) to a final concentration of 5 μM of α-synuclein and their CD spectra were collected on an Applied Photophysics CHIRASCAN PLUS CD Spectrophotometer equipped with a Quantum Northwest TC125 temperature controller at 22 °C using a cell with a 0.2-cm path length. Spectra of protein samples were recorded over a range of 195–260 nm and corrected by subtracting the spectrum of the corresponding solvent, including blank samples of metabolites only. The results were expressed as mean residue ellipticity in deg cm^2 $dmol^{-1}$. CD signal at 218 nm was monitored.

Fluorescent protein-fragment complementation assay

The H4/V1S-SV2 fluorescent protein-complementation assay was used as described previously [69–72]. Briefly, H4 neuroglioma cell line that co-expresses two constructs of α-synuclein, one tagged by the N-terminal half of Venus YFP (V1S) and the other tagged by the C-terminal half of Venus YFP (SV2), both under the tetracycline-controlled transcriptional activation system (Tet-Off induction), was maintained in OPTI-MEM (Gibco) medium supplemented with 10% FBS (Gibco), 200 μg/ml Hygromycin B (Gibco) and 200 μg/ml geneticin (G418; Gibco) in the absence (– Tet) or presence (+ Tet) of 2 μg/ml tetracycline (Tet). Cultured cells in "+ Tet" media were used as baseline. Cells (0.2×10^5) were seeded into each well of a 96-well plate (Corning 4680), with half of the plate cultured in "– Tet" media and the other half in "+ Tet" media and were allowed to adhere overnight at 37 °C. A subset of the wells from both "+ Tet" and "– Tet" cultured media were then treated with pre-formed QA assemblies (at final concentrations of 0.25 and 0.5 mg/ml) and pre-formed α-synuclein fibrils (at final concentration of 0.5 mg/ml) and incubated at 37 °C for 48 h. The whole plate was then stained with Hoechst 33342 (Thermo Fisher Scientific, H3570). Live cells were automatically imaged in the plate using high-content imaging (ImageXpress Micro XLS, Molecular Devices). Nine different non-overlapping fields in each well were automatically selected and imaged. Images were automatically analyzed using the MetaXpress (Molecular Devices) software to measure the number, area and intensity of α-synuclein aggregation. Intensity signals in both "– Tet" and "+ Tet" media were normalized to the number of cells. Average intensities for each condition (no treatment, 0.25 mg/ml of QA assemblies, 0.5 mg/ml of QA assemblies and 0.5 mg/ml of α-synuclein fibrils) in "– Tet" media were normalized with the corresponding "+ Tet" wells. The data points are presented as mean ± SD. The experiment was repeated three times.

Fluorescent labeling of QA assemblies and α-synuclein monomers

QA (11 mg/ml) was dissolved in PBS at 90 °C followed by gradual cooling of the solution. QA assemblies were labeled with a fluorescent dye based on the EDAC (1-ethyl-3-[3-dimethylaminopropyl]carbodiimide hydrochloride) coupling reaction [91]. Briefly, Alexa Fluor 647 Cadaverine (ThermoFisher Scientific, 1 mg) was dissolved in 200 μl of endotoxin-free ultrapure water (Sigma), and 100 μl of resulting solution was added to 570 μl of QA assemblies. Three hundred thirty microliters of freshly prepared EDAC (Sigma) stock solution in PBS was then added to a final concentration of 0.1 M. The sample was incubated for 2 h at room temperature, and the conjugate was purified by overnight dialysis with PBS using a high-throughput dialysis tube (Sigma, 1 kDa MWCO).

A freshly prepared solution of α-synuclein (5 mg/ml) in PBS was labeled with amino-reactive Alexa Fluor 488 NHS Ester (ThermoFisher Scientific) as previously described [66], according to the manufacturer's instructions. Briefly, Alexa Fluor 488 dye (1 mg) was dissolved in 100 μl of DMSO (Sigma), and the resulting solution was added to 500 μl of α-synuclein monomers. Sixty microliters of freshly prepared 1 M sodium bicarbonate buffer (pH 8.3) was then added to the sample. The sample was incubated for 2 h at room temperature, and the conjugate was purified by overnight dialysis with PBS using a high-throughput dialysis tube (Sigma, 1 kDa MWCO).

Co-localization and uptake analysis in cell cultures

H4/V1S-SV2 cells were seeded at 5×10^5 into 35-mm glass-bottomed dishes (ibidi, μ-Dish 35 mm, high Glass Bottom) and cultured for 24 h. After complete adhesion, cells were treated with 0.5 mg/ml of QA-647 assemblies (see "Fluorescent labeling") and were then incubated at 37 °C for 48 h. After washing with trypsin and cold PBS, live cells were stained with Hoechst 33342 (Thermo Fisher Scientific, H3570). Uptake and co-localization of fluorescently labeled QA assemblies with α-synuclein aggregates in live cells

were examined using a Nikon A1R laser scanning confocal system equipped with a 60× objective and analyzed by a Nikon Advanced Research analysis software. Each experiment was repeated three times.

In vitro co-localization

Fibrillization of α-synuclein monomers by QA assemblies and their co-localization was studied by confocal microscopy as previously described [66]. Briefly, α-synuclein monomers labeled with Alexa Flour-488 at a final concentration of 100 μM were incubated with 30% v/v QA-647 (taken from 2 mg/ml stock samples; see "Fluorescent labeling"). In parallel, a sample of α-synuclein alone was similarly incubated. Samples were incubated on an Eppendorf ThermoMixer® C at 37 °C with shaking at 850 rpm for 48 h (a time-point zero control was mixed before the next step). The final products were diluted 1:10 in PBS and 200 μl of the resulting sample were pipetted on a poly-D-Lysine (PDL) coated coverslip (Neuvitro, H-18-1.5-PDL) and incubated at room temperature for 30 min. The solution was then removed, and after washing with PBS, the coverslip was mounted on a microscope slide (Fisher Scientific) using a drop of mounting medium (ibidi). The samples were examined using a Nikon A1R laser scanning confocal system equipped with a 60× objective and analyzed by a Nikon Advanced Research analysis software. Each experiment was repeated three times.

Flow cytometry

SK-N-SH cells were seeded at 1×10^5 per well in 12-well plates in EMEM media supplemented with 10% FBS and penicillin/streptomycin antibiotics and were allowed to adhere overnight at 37 °C. Cells were treated with 0.25 mg/ml of labeled QA-647 assemblies for 24 h and re-plated after washing with trypsin and PBS. Treated and untreated cells were co-cultured for either 72 or 2 h (negative control) in 6-well plates. The cells were then washed with trypsin and PBS, re-suspended in the Live Cell Imaging Solution (ThermoFisher Scientific) and collected in a 96-well plate (300 μl/well). Cells were analyzed by flow cytometry using a single laser-emitting excitation light at 640 nm. Data from 5×10^4 cells were acquired using Guava easyCyte 8HT Benchtop Flow Cytometer and the InCyte Software (Millipore). Analyses were performed using the FlowJo software (TreeStar, version 14). Each experiment was repeated three times.

Acknowledgments

This work was supported by the Israel Science Foundation (grant no. 802/15; E.G.), the Adelis Forever Foundation for E.G., the SAIA Foundation and Prajs-Drimmer Institute for D.S. and the Natural Sciences and Engineering Research Council of Canada (grant 327100-2011) for D.J.V. D.J.V. is supported as a Tier I Canada Research Chair in Chemical Biology. We thank Dr. Pamela J. McLean (Mayo Clinic Florida, Neuroscience, Jacksonville, FL, USA) for providing D.J.V. and O.T. the inducible α-synuclein overexpressing H4 cells for fluorescent protein-fragment complementation assays. We thank the Centre for High-Throughput Chemical Biology at the Simon Fraser University for access to research facilities. We thank Dr. David Levy for support with powder X-ray diffraction and data analysis. We thank Dr. Sasha Lichtenstein for confocal microscopy analysis, Dr. Orit Sagi-Assif for the fluorescence-activated cell sorting analysis, and members of the Gazit group for helpful discussions.

Author Contributions: O.T., D.S., S.S.N. and S.B. performed the experiments. The manuscript was initiated by O.T. and D.S., and compiled and edited by O.T., D.S., D.J.V. and E.G. O.T. and D.S. prepared the graphical items.

Competing Financial Interests: The authors declare no competing financial interest.

Appendix A. Supplementary data

The authors declare that all of the data supporting the findings of this study are available within the article and its Supplementary Information files or from the author upon reasonable request. Supplementary data to this article can be found online at https://doi.org/10.1016/j.jmb.2018.08.002.

Keywords:
metabolite amyloid;
quinolinic acid;
cross-seeding;
α-synuclein;
Parkinson's disease

†O.T. & D.S. contributed equally to this work.

Abbreviations used:
AD, Alzheimer's disease; PD, Parkinson's disease; ACMSD, 2-amino-3-carboxymuconic semialdehyde decarboxylase; PA, picolinic acid; QPRTase, quinolinate phosphoribosyltransferase; TEM, transmission electron microscopy; PXRD, powder X-ray diffraction; EGCG, epigallocatechin gallate; PI, propidium iodide; BSA, bovine serum albumin; CD, circular dichroism; FBS, fetal bovine serum; QA, quinolinic acid.

References

[1] C.A. Ross, M.A. Poirier, Protein aggregation and neurodegenerative disease, Nat. Med. 10 (2004) S10–S17, https://doi.org/10.1038/nm1066.

[2] D. Eisenberg, M. Jucker, The amyloid state of proteins in human diseases, Cell 148 (2012) 1188–1203, https://doi.org/10.1016/j.cell.2012.02.022.

[3] C. Reitz, R. Mayeux, Alzheimer disease: Epidemiology, diagnostic criteria, risk factors and biomarkers, Biochem. Pharmacol. 88 (2014) 640–651, https://doi.org/10.1016/j.bcp.2013.12.024.

[4] L. Petrucelli, D.W. Dickson, Neuropathology of Parkinson's disease, Park. Dis. (2008) 35–48, https://doi.org/10.1016/B978-0-12-374028-1.00003-8.

[5] G.G. Glenner, C.W. Wong, Alzheimer's disease: initial report of the purification and characterization of a novel cerebrovascular amyloid protein, Biochem. Biophys. Res. Commun. 120 (1984) 885–890 (doi:S0006-291X(84)80190-4 [pii]).

[6] A. Kapurniotu, Shedding light on Alzheimer's β-amyloid aggregation with chemical tools, Chembiochem 13 (2012) 27–29, https://doi.org/10.1002/cbic.201100631.

[7] M.G. Spillantini, R.A. Crowther, R. Jakes, N.J. Cairns, P.L. Lantos, M. Goedert, Filamentous alpha-synuclein inclusions link multiple system atrophy with Parkinson's disease and dementia with Lewy bodies, Neurosci. Lett. 251 (1998) 205–208, https://doi.org/10.1016/S0304-3940(98)00504-7.

[8] M. Neumann, D.M. Sampathu, L.K. Kwong, A.C. Truax, M.C. Micsenyi, T.T. Chou, J. Bruce, T. Schuck, M. Grossman, C.M. Clark, L.F. McCluskey, B.L. Miller, E. Masliah, I.R. Mackenzie, H. Feldman, W. Feiden, H.A. Kretzschmar, J.Q. Trojanowski, V.M.-Y. Lee, Ubiquitinated TDP-43 in frontotemporal lobar degeneration and amyotrophic lateral sclerosis, Science 314 (2006) 130–133, https://doi.org/10.1126/science.1134108.

[9] F. Chiti, C.M. Dobson, Protein misfolding, amyloid formation, and human disease: a summary of progress over the last decade, Annu. Rev. Biochem. 86 (2017) 27–68, https://doi.org/10.1146/annurev-biochem-061516-045115.

[10] J.N. Buxbaum, R.P. Linke, A molecular history of the amyloidoses, J. Mol. Biol. 421 (2012) 142–159, https://doi.org/10.1016/j.jmb.2012.01.024.

[11] W. Hwang, S. Zhang, R.D. Kamm, M. Karplus, Kinetic control of dimer structure formation in amyloid fibrillogenesis, Proc. Natl. Acad. Sci. 101 (2004) 12916–12921, https://doi.org/10.1073/pnas.0402634101.

[12] S. Shaham-Niv, L. Adler-Abramovich, L. Schnaider, E. Gazit, Extension of the generic amyloid hypothesis to nonproteinaceous metabolite assemblies, Sci. Adv. 1 (2015), e1500137. https://doi.org/10.1126/sciadv.1500137.

[13] S. Shaham-Niv, P. Rehak, L. Vukovic, L. Adler-Abramovich, P. Kral, E. Gazit, Formation of apoptosis-inducing amyloid fibrils by tryptophan, Isr. J. Chem. 57 (2016) 729–737, https://doi.org/10.1002/ijch.201600076.

[14] L. Adler-Abramovich, L. Vaks, O. Carny, D. Trudler, A. Magno, A. Caflisch, D. Frenkel, E. Gazit, Phenylalanine assembly into toxic fibrils suggests amyloid etiology in phenylketonuria, Nat. Chem. Biol. 8 (2012) 701–706, https://doi.org/10.1038/nchembio.1002.

[15] E. Gazit, Metabolite amyloids: a new paradigm for inborn error of metabolism disorders, J. Inherit. Metab. Dis. 39 (2016) 483–488, https://doi.org/10.1007/s10545-016-9946-9.

[16] E. Gazit, S. Shaham-Niv, P. Rehak, D. Zaguri, A. Levin, L. Adler-Abramovich, L. Vuković, P. Král, Differential inhibition of metabolite amyloid formation by generic fibrillation-modifying polyphenols, Commun. Chem. (2018) 1–11, https://doi.org/10.1038/s42004-018-0025-z (in press).

[17] M.L. Schilsky, Inherited metabolic disease, Curr. Opin. Gastroenterol. 15 (1999) 200–207, https://doi.org/10.1007/978-1-4471-5547-8_45.

[18] W.B. Hanley, Adult phenylketonuria, Am. J. Med. 117 (2004) 590–595, https://doi.org/10.1016/j.amjmed.2004.03.042.

[19] B.G. Anand, K. Dubey, D.S. Shekhawat, K. Kar, Intrinsic property of phenylalanine to trigger protein aggregation and hemolysis has a direct relevance to phenylketonuria, Sci. Rep. 7 (2017) 11146, https://doi.org/10.1038/s41598-017-10911-z.

[20] G. Ragab, M. Elshahaly, T. Bardin, Gout: an old disease in new perspective—a review, J. Adv. Res. 8 (2017) 495–511, https://doi.org/10.1016/j.jare.2017.04.008.

[21] L. Tan, J.T. Yu, L. Tan, The kynurenine pathway in neurodegenerative diseases: mechanistic and therapeutic considerations, J. Neurol. Sci. 323 (2012) 1–8, https://doi.org/10.1016/j.jns.2012.08.005.

[22] M.S. Morris, Homocysteine and Alzheimer's disease, Lancet Neurol. 2 (2003) 425–428, https://doi.org/10.1016/S1474-4422(03)00438-1.

[23] J. Havelund, N. Heegaard, N. Færgeman, J. Gramsbergen, Biomarker research in Parkinson's disease using metabolite profiling, Meta 7 (2017) 42, https://doi.org/10.3390/metabo7030042.

[24] M. Kori, B. Aydın, S. Unal, K.Y. Arga, D. Kazan, Metabolic biomarkers and neurodegeneration: a pathway enrichment analysis of Alzheimer's disease, Parkinson's disease, and amyotrophic lateral sclerosis, OMICS 20 (2016) 645–661, https://doi.org/10.1089/omi.2016.0106.

[25] M.A. Nalls, V. Plagnol, D.G. Hernandez, M. Sharma, U.M. Sheerin, M. Saad, J. Simón-Sánchez, C. Schulte, S. Lesage, S. Sveinbjörnsdóttir, K. Stefánsson, M. Martinez, J. Hardy, P. Heutink, A. Brice, T. Gasser, A.B. Singleton, N.W. Wood, Imputation of sequence variants for identification of genetic risks for Parkinson's disease: a meta-analysis of genome-wide association studies, Lancet 377 (2011) 641–649, https://doi.org/10.1016/S0140-6736(10)62345-8.

[26] I. Ghorayeb, Z. Puschban, P.O. Fernagut, C. Scherfler, R. Rouland, G.K. Wenning, F. Tison, Simultaneous intrastriatal 6-hydroxydopamine and quinolinic acid injection: a model of early-stage striatonigral degeneration, Exp. Neurol. 167 (2001) 133–147, https://doi.org/10.1006/exnr.2000.7535.

[27] G.J. Guillemin, B.J. Brew, C.E. Noonan, O. Takikawa, K.M. Cullen, Indoleamine 2,3 dioxygenase and quinolinic acid immunoreactivity in Alzheimer's disease hippocampus, Neuropathol. Appl. Neurobiol. 31 (2005) 395–404, https://doi.org/10.1111/j.1365-2990.2005.00655.x.

[28] A. Rahman, K. Ting, K.M. Cullen, N. Braidy, B.J. Brew, G.J. Guillemin, The excitotoxin quinolinic acid induces tau phosphorylation in human neurons, PLoS One 4 (2009) 1–15, https://doi.org/10.1371/journal.pone.0006344.

[29] G.K. Wenning, F. Tison, C. Scherfler, Z. Puschban, R. Waldner, R. Granata, I. Ghorayeb, W. Poewe, Towards neurotransplantation in multiple system atrophy: clinical rationale, pathophysiological basis, and preliminary experimental evidence, Cell Transplant. 9 (2000) 279–288.

[30] Y. Chen, G.J. Guillemin, Kynurenine pathway metabolites in humans: disease and healthy states, Int. J. Tryptophan Res. 2 (2009) 1–19, https://doi.org/10.4137/ijtr.s2097.

[31] J.M. Lee, V. Tan, D. Lovejoy, N. Braidy, D.B. Rowe, B.J. Brew, G.J. Guillemin, Involvement of quinolinic acid in the

neuropathogenesis of amyotrophic lateral sclerosis, Neuropharmacology 112 (2017) 346–364, https://doi.org/10.1016/j.neuropharm.2016.05.011.
[32] M.G. Espey, O.N. Chernyshev, J.F. Reinhard, M.A. Namboodiri, C. Colton, Activated human microglia produce the excitotoxin quinolinic acid, Neuroreport 8 (1997) 431–434, https://doi.org/10.1097/00001756-199701200-00011.
[33] G.J. Guillemin, S.J. Kerr, G.A. Smythe, D.G. Smith, V. Kapoor, P.J. Armati, J. Croitoru, B.J. Brew, Kynurenine pathway metabolism in human astrocytes: a paradox for neuronal protection, J. Neurochem. 78 (2001) 842–853, https://doi.org/10.1046/j.1471-4159.2001.00498.x.
[34] M.P. Heyes, C.L. Achim, C.A. Wiley, E.O. Major, K. Saito, S.P. Markey, Human microglia convert L-tryptophan into the neurotoxin quinolinic acid, Biochem. J. 320 (1996) 595–597, https://doi.org/10.1042/bj3200595.
[35] Y. Chen, B.J. Brew, G.J. Guillemin, Characterization of the kynurenine pathway in NSC-34 cell line: implications for amyotrophic lateral sclerosis, J. Neurochem. 118 (2011) 816–825, https://doi.org/10.1111/j.1471-4159.2010.07159.x.
[36] G.J. Guillemin, K.M. Cullen, C.K. Lim, G.A. Smythe, B. Garner, V. Kapoor, O. Takikawa, B.J. Brew, Characterization of the kynurenine pathway in human neurons, J. Neurosci. 27 (2007) 12884–12892, https://doi.org/10.1523/JNEUROSCI.4101-07.2007.
[37] F. Du, E. Okuno, W.O. Whetsell, C. Köhler, R. Schwarcz, Immunohistochemical localization of quinolinic acid phosphoribosyltransferase in the human neostriatum, Neuroscience 42 (1991) 397–406, https://doi.org/10.1016/0306-4522(91)90384-Z.
[38] R.J. Beninger, A.M. Colton, J.L. Ingles, K. Jhamandas, R.J. Boegman, Picolinic acid blocks the neurotoxic but not the neuroexcitant properties of quinolinic acid in the rat brain: evidence from turning behaviour and tyrosine hydroxylase immunohistochemistry, Neuroscience 61 (1994) 603–612, https://doi.org/10.1016/0306-4522(94)90438-3.
[39] B.E. Kalisch, K. Jhamandas, R.J. Boegman, R.J. Beninger, Picolinic acid protects against quinolinic acid-induced depletion of NADPH diaphorase containing neurons in the rat striatum, Brain Res. 668 (1994) 1–8, https://doi.org/10.1016/0006-8993(94)90504-5.
[40] D. Alberati-Giani, P. Ricciardi-Castagnoli, C. Köhler, A.M. Cesura, Regulation of the kynurenine metabolic pathway by interferon-gamma in murine cloned macrophages and microglial cells, J. Neurochem. 66 (1996) 996–1004, https://doi.org/10.1046/j.1471-4159.1996.66030996.x.
[41] K.E. Beagles, P.F. Morrison, M.P. Heyes, Quinolinic acid in vivo synthesis rates, extracellular concentrations, and intercompartmental distributions in normal and immune-activated brain as determined by multiple-isotope microdialysis, J. Neurochem. 70 (1998) 281–291, https://doi.org/10.1046/j.1471-4159.1998.70010281.x.
[42] G.J. Guillemin, G.A. Smythe, L.A. Veas, O. Takikawa, B.J. Brew, A beta 1-42 induces production of quinolinic acid by human macrophages and microglia, Neuroreport 14 (2003) 2311–2315, https://doi.org/10.1097/01.wnr.0000097042.56589.ff.
[43] G.J. Guillemin, Quinolinic acid, the inescapable neurotoxin, FEBS J. 279 (2012) 1356–1365, https://doi.org/10.1111/j.1742-4658.2012.08485.x.
[44] N. Braidy, R. Grant, B.J. Brew, S. Adams, T. Jayasena, G.J. Guillemin, Effects of kynurenine pathway metabolites on intracellular NAD+ synthesis and cell death in human primary astrocytes and neurons, Int. J. Tryptophan Res. 2 (2009) 61–69, https://doi.org/10.4137/IJTR.S2318.
[45] D. Chang, M.A. Nalls, I.B. Hallgrímsdóttir, J. Hunkapiller, M. van der Brug, F. Cai, G.A. International Parkinson's Disease Genomics Consortium, G. 23andMe Research Team, G.A. Kerchner, G. Ayalon, B. Bingol, M. Sheng, D. Hinds, T.W. Behrens, A.B. Singleton, T.R. Bhangale, R.R. Graham, A meta-analysis of genome-wide association studies identifies 17 new Parkinson's disease risk loci, Nat. Genet. 49 (2017) 1511–1516, https://doi.org/10.1038/ng.3955.
[46] C.M. Lill, J.T. Roehr, M.B. McQueen, F.K. Kavvoura, S. Bagade, B.M.M. Schjeide, L.M. Schjeide, E. Meissner, U. Zauft, N.C. Allen, T. Liu, M. Schilling, K.J. Anderson, G. Beecham, D. Berg, J.M. Biernacka, A. Brice, A.L. DeStefano, C.B. Do, N. Eriksson, S.A. Factor, M.J. Farrer, T. Foroud, T. Gasser, T. Hamza, J.A. Hardy, P. Heutink, E.M. Hill-Burns, C. Klein, J.C. Latourelle, D.M. Maraganore, E.R. Martin, M. Martinez, R.H. Myers, M.A. Nalls, N. Pankratz, H. Payami, W. Satake, W.K. Scott, M. Sharma, A.B. Singleton, K. Stefansson, T. Toda, J.Y. Tung, J. Vance, N.W. Wood, C.P. Zabetian, P. Young, R.E. Tanzi, M.J. Khoury, F. Zipp, H. Lehrach, J.P.A. Ioannidis, L. Bertram, Comprehensive research synopsis and systematic meta-analyses in Parkinson's disease genetics: the PDgene database, PLoS Genet. 8 (2012), https://doi.org/10.1371/journal.pgen.1002548.
[47] M. Sharma, J.P.A. Ioannidis, J.O. Aasly, G. Annesi, A. Brice, C. Van Broeckhoven, L. Bertram, M. Bozi, D. Crosiers, C. Clarke, M. Facheris, M. Farrer, G. Garraux, S. Gispert, G. Auburger, C. Vilariño-Güell, G.M. Hadjigeorgiou, A.A. Hicks, N. Hattori, B. Jeon, S. Lesage, C.M. Lill, J.J. Lin, T. Lynch, P. Lichtner, A.E. Lang, V. Mok, B. Jasinska-Myga, G.D. Mellick, K.E. Morrison, G. Opala, P.P. Pramstaller, I. Pichler, S.S. Park, A. Quattrone, E. Rogaeva, O.A. Ross, L. Stefanis, J.D. Stockton, W. Satake, P.A. Silburn, J. Theuns, E.K. Tan, T. Toda, H. Tomiyama, R.J. Uitti, K. Wirdefeldt, Z. Wszolek, G. Xiromerisiou, K.C. Yueh, Y. Zhao, T. Gasser, D. Maraganore, R. Krüger, Large-scale replication and heterogeneity in Parkinson disease genetic loci, Neurology 79 (2012) 659–667, https://doi.org/10.1212/WNL.0b013e318264e353.
[48] J.F. Martí-Massó, A. Bergareche, V. Makarov, J. Ruiz-Martinez, A. Gorostidi, A. López De Munain, J.J. Poza, P. Striano, J.D. Buxbaum, C. Paisán-Ruiz, The ACMSD gene, involved in tryptophan metabolism, is mutated in a family with cortical myoclonus, epilepsy, and parkinsonism, J. Mol. Med. 91 (2013) 1399–1406, https://doi.org/10.1007/s00109-013-1075-4.
[49] D. Vilas, R. Fernández-Santiago, E. Sanchez, L.J. Azcona, M. Santos-Montes, P. Casquero, L. Argandoña, E. Tolosa, C. Paisán-Ruiz, A novel p.Glu298Lys mutation in the ACMSD gene in sporadic Parkinson's disease, J. Park. Dis. 7 (2017) 459–463, https://doi.org/10.3233/JPD-171146.
[50] G.J. Guillemin, B.J. Brew, C.E. Noonan, T.G. Knight, G.A. Smythe, K.M. Cullen, Mass spectrometric detection of quinolinic acid in microdissected Alzheimer's disease plaques, Int. Congr. Ser. 1304 (2007) 404–408, https://doi.org/10.1016/j.ics.2007.07.012.
[51] J.H. Toyn, X.-A. Lin, M.W. Thompson, V. Guss, J.E. Meredith, S. Sankaranarayanan, N. Barrezueta, J. Corradi, A. Majumdar, D.L. Small, M. Hansard, T. Lanthorn, R.S. Westphal, C.F. Albright, Viable mouse gene ablations that robustly alter brain Aβ levels are rare, BMC Neurosci. 11 (2010) 143, https://doi.org/10.1186/1471-2202-11-143.
[52] H. Liu, K. Woznica, G. Catton, A. Crawford, N. Botting, J.H. Naismith, Structural and kinetic characterization of auinolinate phosphoribosyltransferase (hQPRTase) from homo sapiens, J. Mol. Biol. 373 (2007) 755–763, https://doi.org/10.1016/j.jmb.2007.08.043.

[53] D. Sade, S. Shaham-Niv, Z.A. Arnon, O. Tavassoly, E. Gazit, Seeding of proteins into amyloid structures by metabolite assemblies may clarify certain unexplained epidemiological associations, Open Biol. 8 (2018) 170229, https://doi.org/10.1098/rsob.170229.
[54] D. Braconi, L. Millucci, A. Bernini, O. Spiga, P. Lupetti, B. Marzocchi, N. Niccolai, G. Bernardini, A. Santucci, Homogentisic acid induces aggregation and fibrillation of amyloidogenic proteins, Biochim. Biophys. Acta 1861 (2017) 135–146, https://doi.org/10.1016/j.bbagen.2016.11.026.
[55] F. Takusagawa, T.F. Koetzle, IUCr, a refinement of the crystal structure of quinolinic acid at 100 K with neutron diffraction data, Acta Crystallogr. 34 (1978) 1149–1154, https://doi.org/10.1107/S0567740878005117.
[56] M. Biancalana, S. Koide, Molecular mechanism of Thioflavin-T binding to amyloid fibrils, Biochim. Biophys. Acta 1804 (2010) 1405–1412, https://doi.org/10.1016/j.bbapap.2010.04.001.
[57] L.C. Serpell, J.M. Smith, Direct visualisation of the β-Sheet structure of synthetic Alzheimer's amyloid, J. Mol. Biol. 299 (2000) 225–231, https://doi.org/10.1006/jmbi.2000.3650.
[58] T. Eichner, S.E. Radford, A diversity of assembly mechanisms of a generic amyloid fold, Mol. Cell 43 (2011) 8–18, https://doi.org/10.1016/j.molcel.2011.05.012.
[59] A.K. Buell, E.K. Esbjörner, P.J. Riss, D.A. White, F.I. Aigbirhio, G. Toth, M.E. Welland, C.M. Dobson, T.P.J. Knowles, Probing small molecule binding to amyloid fibrils, Phys. Chem. Chem. Phys. 13 (2011) 20044–20052, https://doi.org/10.1039/c1cp22283j.
[60] L.S. Wolfe, M.F. Calabrese, A. Nath, D.V. Blaho, A.D. Miranker, Y. Xiong, Protein-induced photophysical changes to the amyloid indicator dye thioflavin T, Proc. Natl. Acad. Sci. 107 (2010) 16863–16868, https://doi.org/10.1073/pnas.1002867107.
[61] A.I. Sulatskaya, I.M. Kuznetsova, K.K. Turoverov, Interaction of thioflavin T with amyloid fibrils: fluorescence quantum yield of bound dye, J. Phys. Chem. B 116 (2012) 2538–2544, https://doi.org/10.1021/jp2083055.
[62] A.I. Sulatskaya, A.A. Maskevich, I.M. Kuznetsova, V.N. Uversky, K.K. Turoverov, Fluorescence quantum yield of thioflavin T in rigid isotropic solution and incorporated into the amyloid fibrils, PLoS One 5 (2010), e15385. https://doi.org/10.1371/journal.pone.0015385.
[63] S. Grudzielanek, A. Velkova, A. Shukla, V. Smirnovas, M. Tatarek-Nossol, H. Rehage, A. Kapurniotu, R. Winter, Cytotoxicity of insulin within its self-assembly and amyloidogenic pathways, J. Mol. Biol. 370 (2007) 372–384, https://doi.org/10.1016/J.JMB.2007.04.053.
[64] Y.-P. Li, A.F. Bushnell, C.-M. Lee, L.S. Perlmutter, S.K.-F. Wong, β-Amyloid induces apoptosis in human-derived neurotypic SH-SY5Y cells, Brain Res. 738 (1996) 196–204, https://doi.org/10.1016/S0006-8993(96)00733-0.
[65] D.E. Ehrnhoefer, J. Bieschke, A. Boeddrich, M. Herbst, L. Masino, R. Lurz, S. Engemann, A. Pastore, E.E. Wanker, EGCG redirects amyloidogenic polypeptides into unstructured, off-pathway oligomers, Nat. Struct. Mol. Biol. 15 (2008) 558–566, https://doi.org/10.1038/nsmb.1437.
[66] J. Bieschke, J. Russ, R.P. Friedrich, D.E. Ehrnhoefer, H. Wobst, K. Neugebauer, E.E. Wanker, EGCG remodels mature alpha-synuclein and amyloid-beta fibrils and reduces cellular toxicity, Proc. Natl. Acad. Sci. 107 (2010) 7710–7715, https://doi.org/10.1073/pnas.0910723107.
[67] A.K. Buell, C. Galvagnion, R. Gaspar, E. Sparr, M. Vendruscolo, T.P.J. Knowles, S. Linse, C.M. Dobson, Solution conditions determine the relative importance of nucleation and growth processes in α-synuclein aggregation, Proc. Natl. Acad. Sci. 111 (2014) 7671–7676, https://doi.org/10.1073/pnas.1315346111.
[68] R. Shaltiel-Karyo, M. Frenkel-Pinter, N. Egoz-Matia, A. Frydman-Marom, D.E. Shalev, D. Segal, E. Gazit, Inhibiting α-synuclein oligomerization by stable cell-penetrating β-synuclein fragments recovers phenotype of Parkinson's disease model flies, PLoS One 5 (2010), e13863. https://doi.org/10.1371/journal.pone.0013863.
[69] M. López De La Paz, K. Goldie, J. Zurdo, E. Lacroix, C.M. Dobson, A. Hoenger, L. Serrano, De novo designed peptide-based amyloid fibrils, Proc. Natl. Acad. Sci. 99 (2002) 16052–16057, https://doi.org/10.1073/pnas.252340199.
[70] L.C. Serpell, J. Berriman, R. Jakes, M. Goedert, R.A. Crowther, Fiber diffraction of synthetic alpha-synuclein filaments shows amyloid-like cross-beta conformation, Proc. Natl. Acad. Sci. 97 (2000) 4897–4902, https://doi.org/10.1073/pnas.97.9.4897.
[71] S.W. Chen, S. Drakulic, E. Deas, M. Ouberai, F.A. Aprile, R. Arranz, S. Ness, C. Roodveldt, T. Guilliams, E.J. De-Genst, D. Klenerman, N.W. Wood, T.P.J. Knowles, C. Alfonso, G. Rivas, A.Y. Abramov, J.M. Valpuesta, C.M. Dobson, N. Cremades, Structural characterization of toxic oligomers that are kinetically trapped during α-synuclein fibril formation, Proc. Natl. Acad. Sci. 112 (2015) E1994–E2003, https://doi.org/10.1073/pnas.1421204112.
[72] H.-L. Zhu, S.-R. Meng, J.-B. Fan, J. Chen, Y. Liang, Fibrillization of human Tau is accelerated by exposure to lead via interaction with His-330 and His-362, PLoS One 6 (2011), e25020. https://doi.org/10.1371/journal.pone.0025020.
[73] O. Tavassoly, S. Nokhrin, O.Y. Dmitriev, J.S. Lee, Cu(II) and dopamine bind to α-synuclein and cause large conformational changes, FEBS J. 281 (2014) 2738–2753, https://doi.org/10.1111/febs.12817.
[74] P. Jiang, M. Gan, S.-H. Yen, P.J. McLean, D.W. Dickson, Impaired endo-lysosomal membrane integrity accelerates the seeding progression of α-synuclein aggregates, Sci. Rep. 7 (2017) 7690, https://doi.org/10.1038/s41598-017-08149-w.
[75] P. Jiang, M. Gan, S.-H. Yen, S. Moussaud, P.J. McLean, D.W. Dickson, Proaggregant nuclear factor(s) trigger rapid formation of α-synuclein aggregates in apoptotic neurons, Acta Neuropathol. 132 (2016) 77–91, https://doi.org/10.1007/s00401-016-1542-4.
[76] M. Delenclos, T. Trendafilova, D. Mahesh, A.M. Baine, S. Moussaud, I.K. Yan, T. Patel, P.J. McLean, Investigation of endocytic pathways for the internalization of exosome-associated oligomeric alpha-synuclein, Front. Neurosci. 11 (2017) 172, https://doi.org/10.3389/fnins.2017.00172.
[77] S. Moussaud, S. Malany, A. Mehta, S. Vasile, L.H. Smith, P.J. McLean, Targeting α-synuclein oligomers by protein-fragment complementation for drug discovery in synucleinopathies, Expert Opin. Ther. Targets 19 (2015) 589–603, https://doi.org/10.1517/14728222.2015.1009448.
[78] M. Masuda-Suzukake, T. Nonaka, M. Hosokawa, T. Oikawa, T. Arai, H. Akiyama, D.M.A. Mann, M. Hasegawa, Prion-like spreading of pathological α-synuclein in brain, Brain 136 (2013) 1128–1138, https://doi.org/10.1093/brain/awt037.
[79] B. Frost, M.I. Diamond, Prion-like mechanisms in neurodegenerative diseases, Nat. Rev. Neurosci. 11 (2009) 155–159, https://doi.org/10.1038/nrn2786.
[80] J.L. Guo, V.M.Y. Lee, Cell-to-cell transmission of pathogenic proteins in neurodegenerative diseases, Nat. Med. 20 (2014) 130–138, https://doi.org/10.1038/nm.3457.

[81] M. Jucker, L.C. Walker, Self-propagation of pathogenic protein aggregates in neurodegenerative diseases, Nature 501 (2013) 45–51, https://doi.org/10.1038/nature12481.
[82] S. Peled, D. Sade, Y. Bram, Z. Porat, T. Kreiser, M. Mimouni, A. Lichtenstein, D. Segal, E. Gazit, Single cell imaging and quantification of TDP-43 and α-synuclein intercellular propagation, Sci. Rep. 7 (2017) 544, https://doi.org/10.1038/s41598-017-00657-z.
[83] J.F. Havelund, A.D. Andersen, M. Binzer, M. Blaabjerg, N.H.H. Heegaard, E. Stenager, N.J. Faergeman, J.B. Gramsbergen, Changes in kynurenine pathway metabolism in Parkinson patients with L-DOPA-induced dyskinesia, J. Neurochem. 142 (2017) 1–11, https://doi.org/10.1111/jnc.14104.
[84] J.C. Eads, D. Ozturk, T.B. Wexler, C. Grubmeyer, J.C. Sacchettini, A new function for a common fold: the crystal structure of quinolinic acid phosphoribosyltransferase, Structure 5 (1997) 47–58, https://doi.org/10.1016/S0969-2126(97)00165-2.
[85] A. Oueslati, M. Ximerakis, K. Vekrellis, Protein transmission, seeding and degradation: key steps for α-synuclein prion-like propagation, Exp. Neurobiol. 23 (2014) 324–336, https://doi.org/10.5607/en.2014.23.4.324.
[86] D. Kuzdas-Wood, L. Fellner, M. Premstaller, C. Borm, B. Bloem, D. Kirik, G.K. Wenning, N. Stefanova, Overexpression of α-synuclein in oligodendrocytes does not increase susceptibility to focal striatal excitotoxicity, BMC Neurosci. 16 (2015) 86, https://doi.org/10.1186/s12868-015-0227-6.
[87] O. Julien, M. Kampmann, M.C. Bassik, J.A. Zorn, V.J. Venditto, K. Shimbo, N.J. Agard, K. Shimada, A.L. Rheingold, B.R. Stockwell, J.S. Weissman, J.A. Wells, Unraveling the mechanism of cell death induced by chemical fibrils, Nat. Chem. Biol. 10 (2014) 969–976, https://doi.org/10.1038/nchembio.1639.
[88] B.H. Toby, R.B. Von Dreele, GSAS-II: the genesis of a modern open-source all purpose crystallography software package, J. Appl. Crystallogr. 46 (2013) 544–549, https://doi.org/10.1107/S0021889813003531.
[89] H.M. Rietveld, A profile refinement method for nuclear and magnetic structures, J. Appl. Crystallogr. 2 (1969) 65–71, https://doi.org/10.1107/S0021889869006558.
[90] O. Tavassoly, J. Kakish, S. Nokhrin, O. Dmitriev, J.S. Lee, The use of nanopore analysis for discovering drugs which bind to α-synuclein for treatment of Parkinson's disease, Eur. J. Med. Chem. 88 (2014) 42–54, https://doi.org/10.1016/j.ejmech.2014.07.090.
[91] G.T. Hermanson, Zero-Length Cross-linkers, Bioconjugate Tech, Elsevier 1996, pp. 169–186, https://doi.org/10.1016/B978-012342335-1/50004-X.